PNAS RESEARCH ARTICLE | ECOLOGY

Microbial population dynamics decouple growth response from environmental nutrient concentration

Justus Wilhelm Fink[a,1], Noelle A. Held[a,b], and Michael Manhart[a,b,c,1]

Edited by Michael Lynch, Arizona State University, Tempe, AZ; received May 6, 2022; accepted November 22, 2022

How the growth rate of a microbial population responds to the environmental availability of chemical nutrients and other resources is a fundamental question in microbiology. Models of this response, such as the widely used Monod model, are generally characterized by a maximum growth rate and a half-saturation concentration of the resource. What values should we expect for these half-saturation concentrations, and how should they depend on the environmental concentration of the resource? We survey growth response data across a wide range of organisms and resources. We find that the half-saturation concentrations vary across orders of magnitude, even for the same organism and resource. To explain this variation, we develop an evolutionary model to show that demographic fluctuations (genetic drift) can constrain the adaptation of half-saturation concentrations. We find that this effect fundamentally differs depending on the type of population dynamics: Populations undergoing periodic bottlenecks of fixed size will adapt their half-saturation concentrations in proportion to the environmental resource concentrations, but populations undergoing periodic dilutions of fixed size will evolve half-saturation concentrations that are largely decoupled from the environmental concentrations. Our model not only provides testable predictions for laboratory evolution experiments, but it also reveals how an evolved half-saturation concentration may not reflect the organism's environment. In particular, this explains how organisms in resource-rich environments can still evolve fast growth at low resource concentrations. Altogether, our results demonstrate the critical role of population dynamics in shaping fundamental ecological traits.

microbial evolution | Monod model | resource competition | half-saturation concentration | selection–drift balance

Significance

How does the growth rate of microbes depend on the amount of nutrients available? We collect data on this relationship across many different microbial species and nutrients. Our analysis shows that the ability of microbes to grow with scarce nutrients varies widely, even within a single species, and on average does not come at the cost of fast growth with abundant nutrients. Using a mathematical model, we predict how this relationship evolves under different patterns of growth, death, and nutrient supply. Surprisingly, we find that microbes' evolved ability to grow with scarce nutrients does not necessarily reflect the amount of nutrients in their environment. This explains how microbes living with abundant nutrients can still grow rapidly when nutrients become scarce.

Microbial populations rely on a wide range of resources, including chemical nutrients such as sugars, minerals, and metals, as well as space, light, and prey (1). These resources vary in abundance across time and environments, which typically elicits differences in growth rates (2–4). A significant literature discusses how natural populations can be classified as oligotrophs or copiotrophs (4–6), that differ, among other things, in their growth rate response to resource concentration. The most widely used quantitative model of the relationship between growth rate and resource concentration is attributed to Jacques Monod (7). In the Monod model, growth rate increases linearly with resource concentration at low concentrations, and then saturates at high concentrations, reaching half its maximum value at some intermediate concentration of resources. This half-saturation concentration of the growth response, also known as the Monod constant, therefore plays a key role in determining the ability of the population to grow on scarce resources. This suggests that lower resource concentrations in the environment may drive populations to evolve commensurately lower half-saturation concentrations (8, 9), one of the main predictions of resource-ratio theory (10–12). Quantitative models and data for the dependence of growth rate on resource concentration are important both for predicting the behavior of a population under different environmental conditions (13–15) as well as for inferring the natural environmental niche from evolved traits of the population. This inverse approach has been used, for example, to infer separate niches for ammonia-oxidizing archaea and bacteria in the global nitrogen cycle based on kinetic parameters for resource consumption (16–19).

Even though these concepts have been central elements of microbiology and ecology for decades, there is limited experimental evidence that directly demonstrates the evolution of growth rate response to resources. Continuous culture for 200 to 300 generations led to improved growth rates at low glucose concentrations for *Escherichia coli* (20, 21) and *Saccharomyces cerevisiae* (22), but as the genetic changes in these experiments are unknown, the improved growth could not be clearly attributed to mutations (rather than physiological acclimation). The long-term evolution experiment (LTEE) of *E. coli* found that the half-saturation concentration for glucose

Author contributions: J.W.F. and M.M. designed research; J.W.F. and M.M. performed research; J.W.F., N.A.H., and M.M. analyzed data; N.A.H. performed literature survey and assembled resource threshold dataset; and J.W.F. and M.M. wrote the paper.

The authors declare no competing interest.

This article is a PNAS Direct Submission.

Copyright © 2023 the Author(s). Published by PNAS. This article is distributed under Creative Commons Attribution-NonCommercial-NoDerivatives License 4.0 (CC BY-NC-ND).

[1]To whom correspondence may be addressed. Email: justus.fink@env.ethz.ch or mmanhart@rutgers.edu.

This article contains supporting information online at http://www.pnas.org/lookup/suppl/doi:10.1073/pnas.2207295120/-/DCSupplemental.

Published January 4, 2023.

Downloaded from https://www.pnas.org by LIB4RI: EAWAG-EMPA SERIALS DEPARTMENT on March 6, 2023 from IP address 152.88.31.155.

actually increased over the first 2,000 generations, although the maximum growth rate at much higher glucose concentrations significantly increased as well (23). More recently, Bernhardt et al. (12) observed adaptation in the half-saturation concentration for phosphorus of *Chlamydomonas reinhardtii* when limited for phosphorus, but they did not obtain consistent outcomes for nitrogen and light. Perhaps the most explicit evidence so far is from Hart et al. (24), who found that a synthetic auxotroph strain of *S. cerevisiae* significantly reduced its half-saturation concentration for lysine through genetic adaptations.

While laboratory experiments can test the basic principle, mathematical models are better suited to exploring the wide range of environments necessary to establish the link between environment and evolved traits. Previous modeling studies on this topic have focused on how tradeoffs in the growth rate at low versus high resource concentrations define an optimum strategy for a single strain (13) or can facilitate coexistence of multiple strains or species when resource concentrations fluctuate (25, 26). More recent work has shown how this coexistence can spontaneously evolve if such tradeoffs constrain the effects of mutations (27, 28). However, the evidence for these tradeoffs, especially on spontaneous mutations, is limited (27–31). Thus, their importance for explaining the evolved variation in growth rate response, especially the half-saturation concentration, is unclear.

Here, we address this problem using both empirical and modeling approaches. We first perform a survey of data for the growth rate response to resource concentration across a wide range of organisms and resources. We find that the measured half-saturation concentrations vary over orders of magnitude, even within some single species on the same resource, such as *E. coli* strains on glucose. We also find no evidence for tradeoffs between growth rates at low versus high resource concentrations. To better understand the potential causes of this variation, we model evolution for populations with a single limiting resource under feast-and-famine conditions (batch dynamics with fixed biomass or fixed dilution factor) and steady-state growth (chemostat dynamics). We show how demographic fluctuations, known as genetic drift, inhibit selection on lower half-saturation concentration, which leads to a general relationship between the evolved half-saturation concentration, environmental resource concentration, and the effective population size. Using this result, we determine that populations with fixed-bottleneck batch dynamics will evolve half-saturation concentrations that are proportional to the environmental resource concentration, but populations with fixed-dilution batch dynamics evolve half-saturation concentrations that are practically independent of the environment. Besides providing a testable theory for laboratory evolution experiments, our results help to explain how species evolving under high concentrations can maintain fast growth at low concentrations and why evolved half-saturation concentrations may not reflect the environment of origin.

Results

The Monod Model Quantifies Growth Rate Response to Resource Concentration. Consider a population of microbes consuming a resource; we will generally focus on chemical nutrients such as carbon or nitrogen sources, but some aspects of the model apply to other types of resources as well (e.g., prey or light). While microbes consume many different resources simultaneously (32, 33), for simplicity, here, we assume only a single resource limits growth (*SI Appendix*, section S1). The best-known dependence of population growth rate g on resource concentration R is the Monod model (7):

$$g(R) = g^{\max} \cdot \frac{R}{R+K}, \qquad [1]$$

where $g^{\max}$ is the maximum growth rate—achieved when the resource is unlimited—and K is the concentration for the resource at which the growth rate is slowed to half its maximum (Fig. 1). Decreasing the half-saturation concentration K therefore allows the population to grow faster at lower resource concentrations. The half-saturation concentration K is not to be confused with a related but distinct concept of R^* from resource-ratio theory (10, 12). Note that the Monod model of Eq. **1** is used to describe both steady state (12) and nonsteady state (25, 28) relationships between growth rate and environmental resource concentration. While there are many alternative models of how growth rate depends on resource concentration (*SI Appendix*, section S2 and Table S1), we focus on the Monod model due to its wider usage and available data.

The parameter K is sometimes labeled as the affinity for the resource (34), but this is potentially misleading as K is inversely proportional to the ability to grow on the resource. We instead use the term specific affinity to refer to the parameter combination $g^{\max}/K$, which measures how much the growth rate increases per unit change in resource concentration, starting from a low concentration (35). The specific affinity is therefore a common measure for oligotrophic growth ability (9, 16, 19, 34). Note that both K and $g^{\max}$ are required to fully characterize the growth rate dependence; for example, the specific affinity $g^{\max}/K$ alone does not suffice because while it describes the growth rate response at low concentrations, it does not define the range of low concentrations (which is determined separately by K). Since we are primarily interested in how these traits evolve in relation to the environmental concentration R, we focus primarily on the half-saturation concentration K since one can directly compare it to R.

One can derive the Monod model of Eq. **1** by modeling biomass growth as a two-step process, in which uptake of the

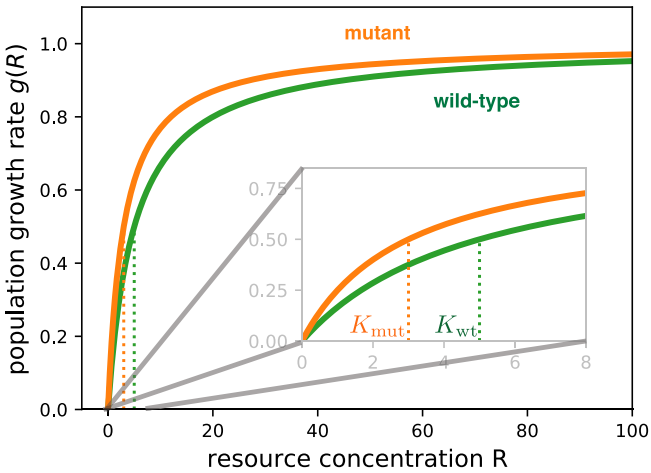

Fig. 1. Monod model of growth rate response to resource concentration. The population growth rate $g(R)$ as a function of the external resource concentration R for two hypothetical strains: a wild-type (green) and a derived mutant strain (orange), with equal maximum growth rates ($g^{\max} = 1$) but different half-saturation concentrations ($K_{wt} = 5$, $K_{mut} = 3$). The *Inset* shows a magnified view at low concentrations near K_{wt} and K_{mut} (dotted vertical lines). Note that the growth rates do not fully overlap at the highest concentration shown but eventually converge to the same value $g^{\max}$ outside the range of this plot.

Downloaded from https://www.pnas.org by LIB4RI: EAWAG-EMPA SERIALS DEPARTMENT on March 6, 2023 from IP address 152.88.31.155.

external resource into the cell occurs at a rate proportional to the external concentration R (36). However, the dependence of growth rate on resource concentration expressed by Eq. **1** is surprisingly robust to additional model complexities (37, 38), albeit with the resulting traits g^{max} and K being emergent properties of whole cells or populations. In particular, the half-saturation concentration K is not equivalent to the Michaelis–Menten constant for resource uptake kinetics (37, 39, 40), despite the mathematical similarity between the Michaelis–Menten and Monod models (Eq. **1**); this is because the Monod model describes the whole process of producing new biomass, of which uptake is just one step.

Half-Saturation Concentrations Vary Widely Across Resources and Organisms. To explore the diversity of microbial growth responses, we have compiled 247 measurements of half-saturation concentrations K from previously published studies (*Methods*, Dataset S1, and *SI Appendix*, Fig. S1), substantially extending previous surveys (41–44). Fig. 2*A* shows an overview of this data, sorted by resource. The data include a wide range of resources, with phosphate, glucose, and nitrate having the largest number of measurements due to their emphasis in marine and laboratory systems. Organisms include prokaryotes and eukaryotes as well as autotrophs and heterotrophs (marked by different symbols in Fig. 2*A*).

Measured values of the half-saturation concentration K vary over several orders of magnitude, ranging from below 10^{-6} μM (for thiamine and vitamin B12) to above 10^{4} μM (for one glucose measurement). This variation is not attributable to measurement uncertainties, which never exceeded 20% in the studies that reported them. It also is not an artifact of technical aspects of the measurements (*SI Appendix*, Fig. S2) such as temperature (linear regression, $R^2 \approx 0.089$, $P \approx 1.2 \times 10^{-5}$) or experimental method (linear regression, $R^2 \approx 0.160$, $P \approx 1.3 \times 10^{-3}$),

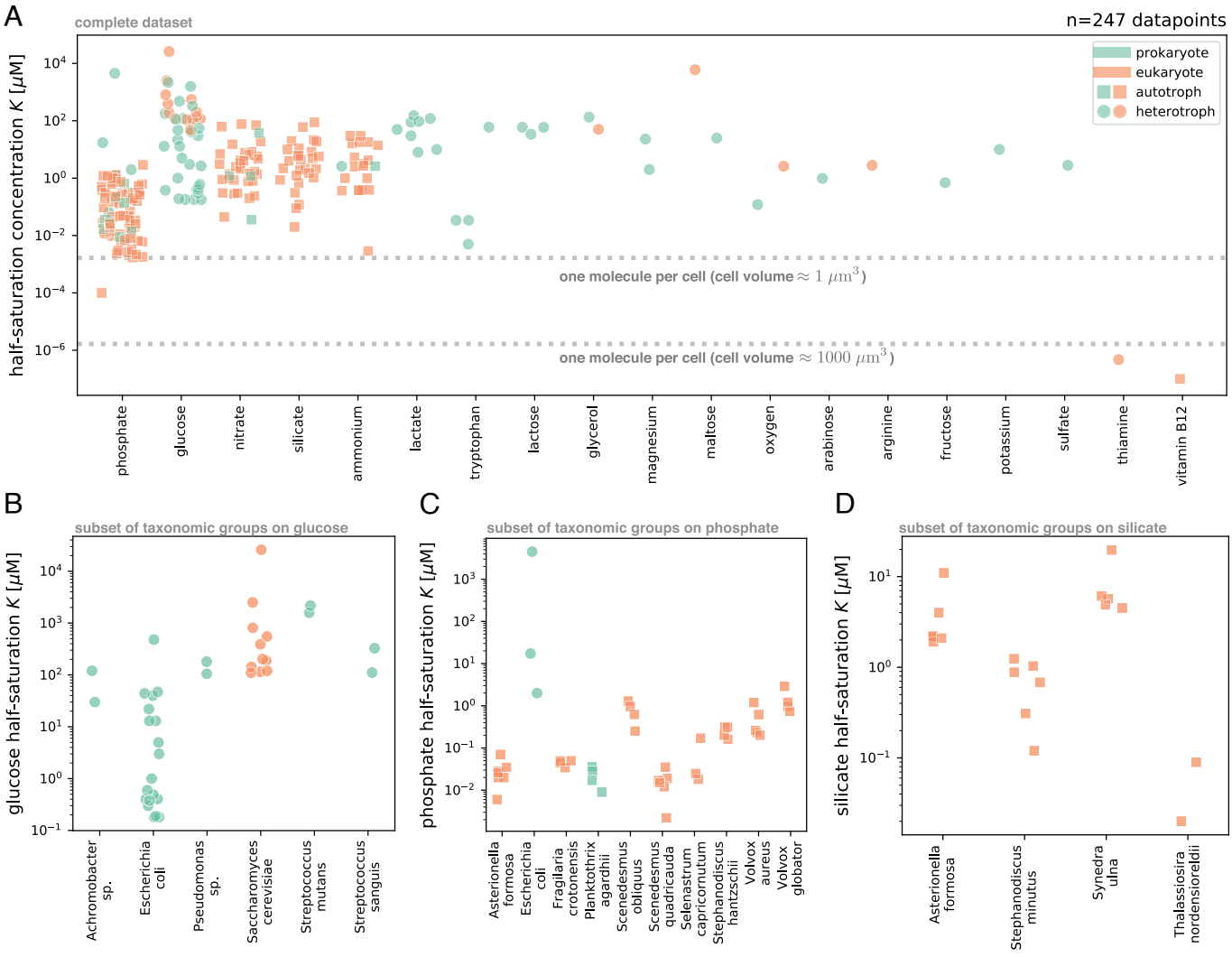

Fig. 2. Survey of measured half-saturation concentrations. (*A*) Complete set of half-saturation concentrations K for the Monod model of growth rate (Eq. **1**) in our survey, grouped by resource (in decreasing order of number of data points). Each point represents a different measurement; color indicates whether the organism is a prokaryote (green) or eukaryote (orange), and shape indicates whether the organism can grow as an autotroph (square) or only as a heterotroph (circle). Dashed lines mark concentrations of one molecule per cell for approximate prokaryotic and eukaryotic cell volumes (45). (*B*) Subset of K measurements from panel *A* for glucose, grouped by taxon (only those with at least two measurements). We use the taxonomic identity given in the original publications, where an ending in sp. means that the isolate is a representative of the genus but was not identified at the species level. Symbols are the same as in panel *A*. For brevity, we use "glucose half-saturation" to refer to the half-saturation concentration for glucose as the limiting nutrient. (*C*) Subset of K measurements from panel *A* for phosphate, grouped by taxon (with at least three measurements). (*D*) Subset for silicate, grouped by taxon (with at least two measurements). *SI Appendix* for additional plots with K measurements for nitrate (*SI Appendix*, Fig. S4*A*) and ammonium (*SI Appendix*, Fig. S4*B*).

Downloaded from https://www.pnas.org by LIB4RI: EAWAG-EMPA SERIALS DEPARTMENT on March 6, 2023 from IP address 152.88.31.155.

nor does the variation appear to be systematically biased by experimental design such as the degree of preacclimation to the growth medium (*SI Appendix*, Fig. S3). We furthermore find no evidence for a major bias from simultaneous limitation (colimitation) for other resources besides the focal resource (*SI Appendix*, section S1).

Instead, most variation of concentrations K corresponds to variation in the identity of the organisms and resources themselves (*SI Appendix*, Fig. S2*A*). Fig. 2*B* shows a subset of measurements on glucose, which have systematic differences in K between taxa. For example, measurements of *S. cerevisiae* and *Streptococcus* almost all have K values higher than those of *E. coli* (Mann–Whitney U test, $P \approx 1.40 \times 10^{-6}$). Phosphate and silicate similarly show significant variation between species (Fig. 2*C* and *D*), as do nitrate and ammonium (*SI Appendix*, Fig. S4). Even within some taxa, there is large variation of K; glucose K in *E. coli* varies over four orders of magnitude (Fig. 2*B*). This variation within a single resource and taxon does not appear to be explained by technical covariates of the measurements (*SI Appendix*, Fig. S2*B*) but rather corresponds to genetically distinct strains of *E. coli* (*SI Appendix*, Fig. S5), suggesting that even subspecies-level genetic variation can lead to significant differences in the half-saturation concentration K. Indeed, Ferenci (46) reported single-target genes, like the membrane-associated lamB or the stress-factor rpoS, that affect the half-saturation concentration of *E. coli* on glucose when mutated. The genetic differences in our dataset are mostly unknown, but we grouped *E. coli* measurements by strain labels to find reproducible half-saturation concentrations for glucose within strains (e.g., ML 30, *SI Appendix*, Fig. S5*A*).

How can we explain this wide variation in half-saturation concentrations? Intuitively, we expect evolution to reduce K since mutations that reduce K increase growth rate (Eq. **1**). For example, Fig. 1 shows the growth rate dependence for a hypothetical wild-type strain (green line) and a mutant (orange) with lower half-saturation K. Since the mutant has a greater relative growth rate advantage at low resource concentrations, there could be stronger selection pressure to reduce K at those low concentrations. This is hinted by some patterns in the data: for example, *E. coli* often grows in mammalian large intestines where there are few simple sugars such as glucose, while *S. cerevisiae* and *Streptococcus* often grow in high-sugar environments (fruit and the oral microbiome, respectively) (47, 48), which could explain their large difference in half-saturation concentrations for glucose.

Variation in Specific Affinity Has Trends Similar to Those of the Half-Saturation Concentration. Since K alone does not define the growth rate at low resource concentrations, it is essential to consider the maximum growth rate $g^{\max}$ or specific affinity $g^{\max}/K$ as well. We show the variation in maximum growth rate $g^{\max}$ across resources in Fig. 3*A* (reported for 97.6% of all entries for half-saturation concentrations K; Dataset S1). The most striking feature of these data is that while maximum growth rates $g^{\max}$ vary less between resources than do half-saturation concentrations K (compare Figs. 3*A* and 2*A*), there is a clear bimodality between fast-growing heterotrophs (circles) and slow-growing autotrophs (squares). Indeed, a closer look at the covariation between $g^{\max}$ and K in autotrophs (squares in Fig. 3*B*) reveals that resources have comparable distributions of $g^{\max}$ but stratify in terms of half-saturation concentrations K, with the lowest values for phosphate. In particular, the distributions for phosphate and nitrate are indistinguishable in terms of maximum growth rate (Mann–Whitney U test, $P = 0.080$) but clearly different in terms of half-saturation concentration (Mann–Whitney U test, $P = 1.28 \times 10^{-12}$). Also, the species differences in maximum growth rate on glucose and phosphate are less pronounced (*SI Appendix*, Fig. S6), and more of the variation can be explained by experiment temperature (*SI Appendix*, Figs. S7 and S8) compared to variation in K.

We can also compute the specific affinity $g^{\max}/K$ for each data point. *SI Appendix*, Fig. S9 shows that the variation in specific affinity is similar to variation in K: The variation spans orders of magnitude, even for single species, and there are systematic differences between taxa (e.g., *E. coli* compared to *S. cerevisiae* and *Streptococcus*; Mann–Whitney U test, $P \approx 1.20 \times 10^{-6}$; *SI Appendix*, Fig. S9*B*). The similarity in patterns of variation between the half-saturation concentration and specific affinity is because variation in $g^{\max}/K$ is dominated by variation in K (*SI Appendix*, Fig. S7*B*); on a logarithmic scale, $g^{\max}/K$ depends on additive contributions from $g^{\max}$ and K, and variation in K is much larger than variation in $g^{\max}$ (compare Figs. 2*A* and 3*A*).

There Is No Evidence for a Tradeoff Between Half-Saturation Concentration and Maximum Growth Rate. Many previous studies have considered the possibility of tradeoffs between $g^{\max}$ and K (positive correlation), such that genotypes growing faster with abundant resources will grow slower when resources are scarce (13, 25–28). If this were true, evolution at high resource concentrations may select for increasing maximum growth rate $g^{\max}$ at the expense of the half-saturation concentration K, leading to high values of K. If we consider all organisms and resources in our data set, we do find a significant positive correlation between $g^{\max}$ and K (Spearman $\rho \approx 0.39$, $P \approx 5.7 \times 10^{-10}$; Fig. 3*B*). However, this correlation is an artifact of the biased sampling of organism–resource pairs, which are dominated by fast-growing heterotrophs on glucose (which tend to have higher concentrations K) and slow-growing autotrophs on other resources (which tend to have lower concentrations K compared to glucose); the correlation disappears when we separate heterotrophs (*SI Appendix*, Fig. S10 *A* and *B*) from autotrophs (*SI Appendix*, Fig. S10 *C* and *D*). If we further separate individual resources, we see no significant correlations for phosphate, nitrate, ammonium, or glucose across organisms (Fig. 3 *C* and *D* and *SI Appendix*, Fig. S10 *E–H*), while there is actually a negative correlation (opposite of a tradeoff) for silicate $g^{\max}$ and K (Spearman $\rho \approx -0.56$, $P \approx 0.0025$; Fig. 3*E*). In Fig. 3*F*, we test the covariation of $g^{\max}$ with K for two individual species (*E. coli* and *S. cerevisiae*) for a single resource (glucose). The *E. coli* data show a positive correlation indicative of a tradeoff, but it has modest magnitude and low statistical significance (Spearman $\rho \approx 0.26$, $P \approx 0.26$). *Saccharomyces cerevisiae*, on the other hand, shows a negative correlation between the two traits (Spearman $\rho \approx -0.75$, $P \approx 0.008$). The lack of tradeoff appears irrespective of experimental method (i.e., batch or chemostat; *SI Appendix*, Fig. S3*B*) and also holds when comparing the maximum growth rate $g^{\max}$ to the specific affinity $g^{\max}/K$ (*SI Appendix*, Fig. S11).

Much of the previous literature arguing for tradeoffs in these traits based their evidence on measurements for resource uptake kinetics (27, 28, 30, 49) rather than on population growth as we consider here. However, we find little to no correspondence between traits of uptake kinetics with traits of population growth in data points where we have measurements for both (*SI Appendix*, Fig. S12) (44), consistent with previous analyses (37, 39). It is therefore not surprising that the observed tradeoffs in uptake do not translate to tradeoffs in growth. For example, Litchman et al. (30) reported a tradeoff between uptake

Downloaded from https://www.pnas.org by LIB4RI: EAWAG-EMPA SERIALS DEPARTMENT on March 6, 2023 from IP address 152.88.31.155.

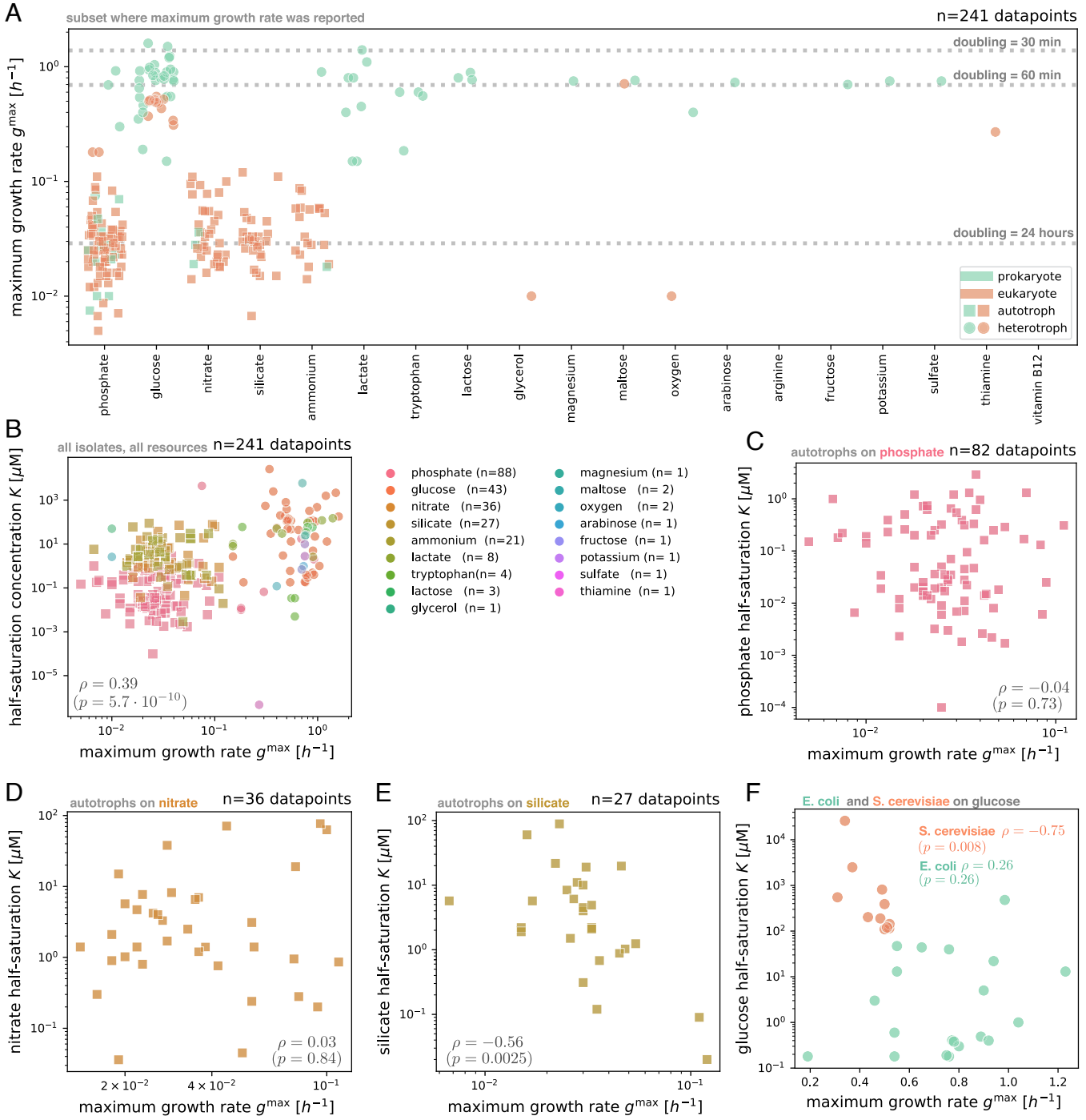

Fig. 3. Survey of maximum growth rates and trait correlations. (*A*) Empirical maximum growth rates g^{max} for the microbial isolates in our survey. There are slightly fewer data points for maximum growth rate compared to half-saturation concentrations in Fig. 2*A* since some publications reported only the half-saturation concentration. Markers indicate whether the organisms can grow as an autotroph (square) or only as a heterotroph (circle); colors indicate whether the isolate is prokaryotic (green) or eukaryotic (orange). Dashed lines mark reference doubling times. (*B*) Covariation of maximum growth rate g^{max} and half-saturation concentration K across the entire set of isolates from panel *A*. Here colors indicate the limiting resource, with the number of measurements n given in parentheses. Marker shapes (squares are autotrophs; circles are heterotrophs) are the same as in panel *A*. We compute the Spearman rank correlation ρ and *P*-value across the pooled set of isolates. (*C*) Subset of measurements from panel *B* for phosphate (only autotroph isolates shown). (*D*) Subset of measurements from panel *B* for nitrate. (*E*) Subset of measurements from panel *B* for silicate. (*F*) Covariation between maximum growth rate g^{max} and half-saturation concentration K on glucose for measurements of *E. coli* (green) and *S. cerevisiae* (orange), with Spearman rank correlations ρ and *P*-values by species.

traits for nitrate, but we see no correlation in growth traits for nitrate (Spearman $\rho \approx 0.03$, $P \approx 0.84$; Fig. 3*D* and *SI Appendix*, Fig. S11*C*). Altogether, the absence of evidence for a systematic correlation between K and g^{max} suggests that selection for g^{max} does not explain the evolved variation in K.

Models of Population Dynamics with Mutations to Half-Saturation Concentration. To test how the environmental resource concentration shapes the evolution of the half-saturation concentration K, we turn to a model of population dynamics with mutations altering traits of the Monod growth rate response

Downloaded from https://www.pnas.org by LIB4RI: EAWAG-EMPA SERIALS DEPARTMENT on March 6, 2023 from IP address 152.88.31.155.

(*Methods*, *SI Appendix*, sections S3–S5, and Table S2). We consider a microbial population consisting of a wild-type and a mutant, with biomasses $N_{wt}(t)$ and $N_{mut}(t)$ that vary over time t. They grow at rates depending on the resource concentration R according to the Monod model (Eq. **1**), but with potentially different values of the traits g^{max} and K depending on the effect of the mutation (25, 28). The rate at which the mutant increases or decreases in frequency compared to the wild-type is given by the selection coefficient s (*SI Appendix*, section S6) (50, 51). We show that s decomposes into two additive terms:

$$s \approx s_{high} + s_{low}, \quad [2]$$

where s_{high} measures selection on growth at high resource concentrations and is therefore proportional to variation in the maximum growth rate g^{max}, while s_{low} measures selection on growth at low resource concentrations and is therefore proportional to variation in the half-saturation concentration K (*SI Appendix*, Figs. S13–S16 and sections S7–S9).

We consider selection in three prototypical regimes of population dynamics. In the first case, the population grows as a batch culture with serial transfers (*SI Appendix*, section S3). That is, there is an initial concentration R_0 of the resource, and the population grows until the resource is exhausted. Fig. 4*A* shows these dynamics for the hypothetical wild-type and mutant strains of Fig. 1. Although the mutant has the same maximum growth rate g^{max} as the wild-type, its lower value of K allows it to continue growing fast at lower concentrations of the resource, decelerating more abruptly at the end of growth (see *Inset* of Fig. 4*A* for more dramatic examples). Then, a fixed amount of biomass N_0—sampled from the whole culture, so that the relative frequencies of the mutant and wild-type are preserved on average—is transferred to a new environment with the same initial concentration R_0 of the resource as before, and the cycle repeats (Fig. 4 *B*, *Top*). This dilution step represents a form of mortality for the population. We refer to this regime as fixed-bottleneck batch dynamics since the bottleneck of biomass between transfers is held fixed. Boom-bust dynamics such as these are believed to be common in some natural environments (52, 53), with a fixed bottleneck size being plausible for populations that serially colonize new environments (54) or are reset to a fixed density by culling (4) between cycles of growth.

The second regime is the same as the first, except instead of transferring a fixed amount of biomass to the next cycle, we transfer a fixed fraction $1/D$, where D is the dilution factor (Fig. 4 *B*, *Bottom*); we therefore refer to this regime as fixed-dilution batch dynamics. Note that the dilution factor D and the bottleneck biomass N_0 are related according to $D = R_0 Y/N_0 + 1$, where Y is the yield (biomass produced per unit resource; *SI Appendix*, section S3). These dynamics are plausible for populations that experience a constant death rate between growth cycles or are regularly purged by the environment, as believed to occur in the human gut microbiome (55). This case is also the most common protocol in laboratory evolution experiments owing to its simplicity (56). While the differences between these two regimes of batch dynamics may appear to be subtle (comparing the two panels of Fig. 4*B*), we will show later that these two dilution protocols have different dependences on the resource concentration, which lead to different evolutionary outcomes.

Finally, we also consider the regime of chemostat dynamics, where the population grows as a continuous culture with a constant supply of the resource and a constant dilution rate d (*SI Appendix*, section S5). Chemostats are used as devices for experimental evolution (12, 22), and the same dynamics are often applied to describe natural populations in the ocean (13, 57).

Selection Quantifies Variation in Growth Traits Between Isolates at Different Resource Concentrations. We previously observed wide variation in half-saturation concentrations K (Fig. 2*A*) and maximum growth rates g^{max} (Fig. 3*A*) across isolates, but the significance of this variation is difficult to assess by itself. For example, glucose K for *E. coli* varied across four orders of magnitude, but how significant is this variation for evolution? Our model of selection under different population dynamics gives us precisely the metric to quantify this variation. We

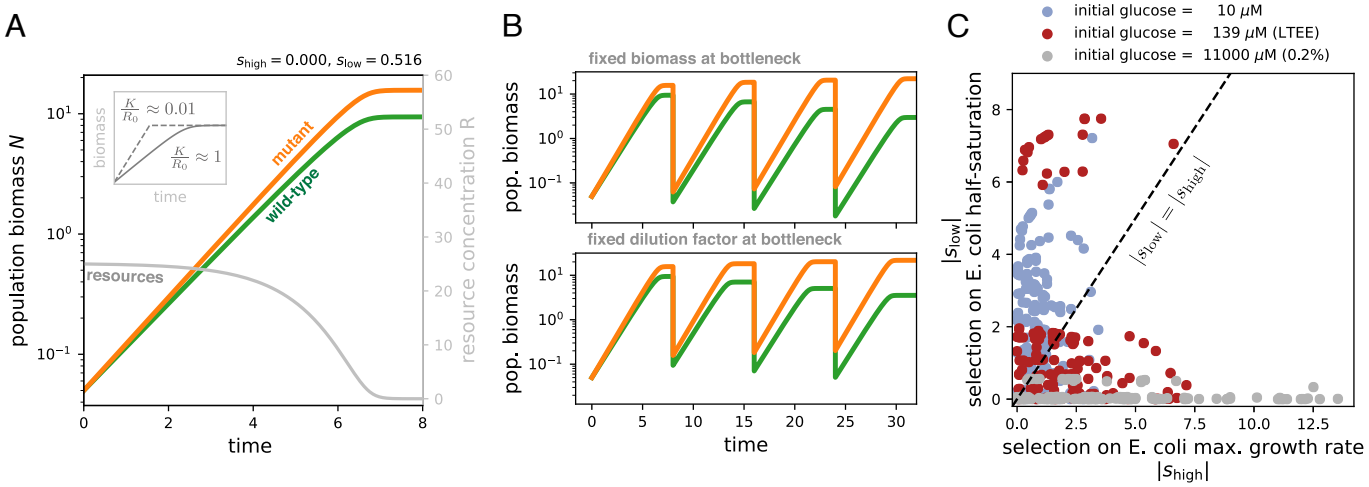

Fig. 4. Selection on variation in half-saturation concentrations over batch population dynamics. (*A*) Simulated growth of wild-type (green) and mutant (orange) strains competing under batch dynamics, with the transient resource concentration (gray) on the right vertical axis (*SI Appendix*, section S3). The strain pair is the same as in Fig. 1; the initial resource concentration is $R_0 = 25$, with strains at equal initial frequencies and equal yields. (*B*) The same strain competition from panel *A* continued over multiple growth cycles under fixed-bottleneck batch dynamics (*Top*, $N_0 = 0.1$) and fixed-dilution batch dynamics (*Bottom*, $D = 100$). (*C*) Each point represents the predicted selection coefficients $|s_{high}|$ and $|s_{low}|$ (Eq. **2** and *SI Appendix*, section S8) for pairs of *E. coli* isolates with measured growth traits on glucose (from Fig. 2*D*). The three colors represent different glucose concentrations. We assume the isolates in each pair start competing at equal initial frequencies, set the initial cell density to $N_0 = 4.6 \times 10^5$ cells/mL, and use a biomass yield of $Y = 3.3 \times 10^8$ cells/μmol glucose measured by a previous study (23).

Downloaded from https://www.pnas.org by LIB4RI: EAWAG-EMPA SERIALS DEPARTMENT on March 6, 2023 from IP address 152.88.31.155.

demonstrate this in Fig. 4*C* by calculating the two components of selection (Eq. **2**) for hypothetical competitions between all pairs of *E. coli* isolates measured on glucose. We do this for batch dynamics starting at different initial concentrations R_0 of glucose. While selection on variation in $g^{\max}$ (s_{high}) always increases with higher R_0, selection on variation in K (s_{low}) depends nonmonotonically on the concentration R_0, such that selection is maximized at some intermediate concentration (*SI Appendix*, Fig. S17 and section S10). Intuitively, this optimal concentration approximately equals the half-saturation concentration K itself (*SI Appendix*, Fig. S17*C*). On the other hand, if the resource concentration R_0 also increases the initial population size N_0 (i.e., transfer from a pregrowth cycle with fixed dilution factor), selection on variation in K depends monotonically on R_0 and is maximized at the lowest concentration (*SI Appendix*, Fig. S18).

We calculate selection between *E. coli* isolates at 10 μM glucose, which is in the middle of the range of observed half-saturation concentrations K, as well as at two higher concentrations corresponding to the conditions of the *E. coli* LTEE (139 μM) (58) and a common laboratory concentration (11,000 μM ≈ 0.2% w/v). Fig. 4*C* indeed shows that variation in the value of K is highly significant for evolution at concentrations around the half-saturation concentration, whereas at the highest concentration, selection on the variation in K is small compared to the selection in $g^{\max}$.

The Half-Saturation Concentration Evolves Downward Over Successive Mutations. With our model of population dynamics, we can predict how the traits of the Monod growth rate response (Eq. **1**) will evolve over long times. For simplicity, we focus on the "strong-selection weak-mutation" (SSWM) regime of evolutionary dynamics, where each new mutation either fixes or goes extinct before the next mutation arises (*SI Appendix*, Fig. S19 and section S11) (59).

We first simulate a population growing under fixed-bottleneck batch dynamics, with an initial half-saturation concentration K that is higher than the external resource concentration R_0; the population therefore decelerates gradually into starvation over each growth cycle (Fig. 5 *A*, *Left Inset*). Mutations then regularly arise and alter the value of K with a random effect size (*SI Appendix*, Fig. S19 and section S11). Each mutation stochastically fixes or goes extinct according to a fixation probability, which depends on the mutation's selection coefficient. Over time, these beneficial mutations accumulate, and the half-saturation concentration K systematically decreases. By the end of the simulation, the half-saturation concentration K is 1,000 times smaller than the resource concentration R_0, leading to growth curves that grow much faster and abruptly decelerate into starvation (Fig. 5 *A*, *Right Inset*).

Such an abrupt arrest is, for example, realized by *E. coli* in glucose-limited batch culture through a dynamic surge in gene expression late in the growth cycle (60), often involving the use of separate transporters with lower Michaelis–Menten constants (61). The presence of these transporter systems has been raised as evidence for evolutionary adaptation of the species at micromolar glucose concentrations (8, 61, 62). But our model shows that a feast-and-famine environment dominated by concentrations orders of magnitude higher would still allow *E. coli* to evolve the low half-saturation concentrations K observed in existing strains.

Adaptation in the Half-Saturation Concentration Stalls When It Reaches Selection–Drift Balance. The value of K does not evolve downward forever; in Fig. 5*A*, adaptation slows down, and the half-saturation concentration levels off after a few tens of thousands of mutations, even though there is no change in the supply of beneficial mutations. This occurs because selection on beneficial mutations is inhibited by random demographic fluctuations in the population, known as genetic drift (63). The strength of genetic drift is measured by $1/N_e$, where N_e is the effective population size (for the variance in mutant frequency change per unit time) (64, 65); smaller populations experience greater fluctuations. In the simplest cases, N_e is proportional to the actual ("census") population size but in more complex systems N_e may depend on other aspects of demography (such as spatial dynamics (66) or age structure (67)) as well as additional sources of noise in the population dynamics (68).

Beneficial mutations will therefore no longer fix with high probability if their selection equals genetic drift, a condition known as selection–drift balance (69–71):

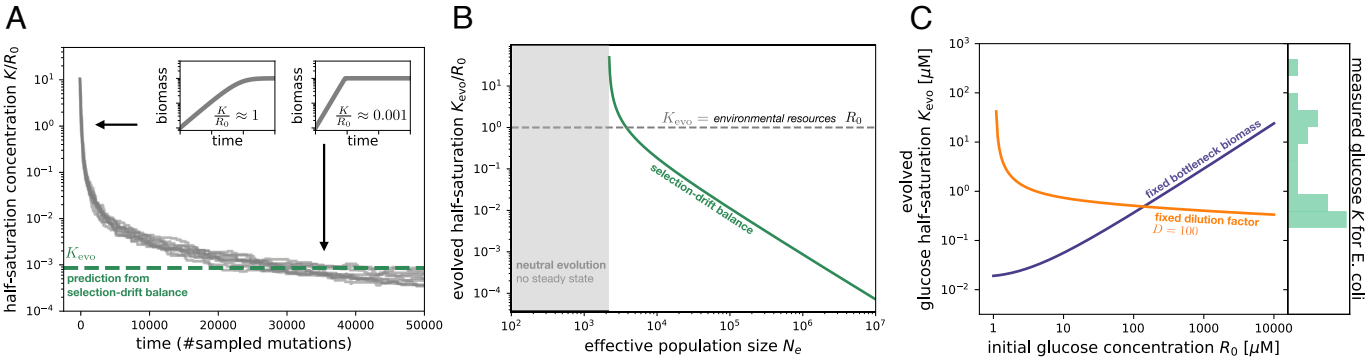

Fig. 5. Evolution of the half-saturation concentration. (*A*) Half-saturation concentration K evolving under fixed-bottleneck batch dynamics. Each gray line is one of 10 independent stochastic simulations using an effective population size $N_e = 1,000$ and mutation effects κ drawn from a uniform distribution (*SI Appendix*, section S11). The *Insets* show the growth curve in a single batch cycle before adaptation (*Left Inset*) and at the final state (*Right Inset*). The green dashed line marks our prediction K_{evo} at selection–drift balance. (*B*) Evolved half-saturation concentration K_{evo} as a function of the effective population size N_e. In the gray region, the effective population size is too small, and all evolution is neutral. If N_e is sufficiently large (white region), the evolved half-saturation K_{evo} is at selection–drift balance along the green line. Parameters are $|\kappa_{\max}| = 0.0001$, $g^{\max} = 1$, $N_0 = 0.01$, and $Y = 1$ for both panels. (*C*) The evolved glucose half-saturation K_{evo} as a function of initial glucose concentration R_0 for two regimes of batch dynamics: fixed-bottleneck dynamics (blue line) and fixed-dilution dynamics (orange line). We use parameters based on the LTEE: $N_0 = 4.6 \times 10^5$ cells/mL (for fixed-bottleneck case), $D = 100$ (for fixed-dilution case), $N_e = VN_0$, where $V = 10$ mL, $g^{\max} = 0.888$/h, and $Y = 3.3 \times 10^8$ cells/μmol (23). We also set $\kappa_{\max} = -6 \times 10^{-6}$ (*SI Appendix*, Fig. S27). On the right axis is a histogram of glucose half-saturation K data for *E. coli* isolates (from Fig. 2*B*).

Downloaded from https://www.pnas.org by LIB4RI: EAWAG-EMPA SERIALS DEPARTMENT on March 6, 2023 from IP address 152.88.31.155.

$$s = \frac{1}{N_e}. \quad [3]$$

Selection–drift balance occurs in our model under batch dynamics because the growth deceleration phase becomes shorter as K decreases over evolution (*Insets* of Figs. 4 *A* and 5 *A*), which means that there is weaker selection to reduce it further. Once the half-saturation concentration K becomes sufficiently small, selection is no longer strong enough to overcome genetic drift (*SI Appendix*, section S12 and Fig. S20).

By combining Eqs. **2** and **3**, we can calculate the value of the evolved half-saturation concentration at which selection–drift balance occurs (*SI Appendix*, Fig. S21). For typical regimes of the parameters, the evolved concentration is approximately (*SI Appendix*, section S13).

$$K_{evo} \approx \frac{R_0}{N_e|\kappa_{max}| \log(N_e|\kappa_{max}|R_0 Y/N_0)}, \quad [4]$$

where κ_{max} is the maximum effect size of a beneficial mutation reducing K. We calculate an example of K_{evo} in Fig. 5*A* (dashed green line), which corresponds well with the simulations. This result is robust to a wide range of effective population sizes and frequency-dependent effects (*SI Appendix*, Fig. S22 and section S11). We also observe an equivalent result for the adaptation of the specific affinity g^{max}/K (*SI Appendix*, Fig. S23 and section S14) instead of the half-saturation concentration K alone.

One salient feature of Eq. **4** is that the evolved half-saturation concentration K_{evo} scales inversely with the effective population size N_e, as shown in Fig. 5*B*. That is, larger populations or those with lower genetic drift can evolve proportionally lower half-saturation concentrations K_{evo} that are orders of magnitude lower than the environmental resource concentration R_0. This potentially explains why we observe such low values of K for many organisms and resources (Fig. 2); this also explains why these half-saturation concentrations are difficult to measure from time-series data since low half-saturation concentrations produce extremely abrupt deceleration at the end of growth (*Insets* of Figs. 4 *A* and 5 *A* and *SI Appendix*, Fig. S24 and section S15). Hints of the influence of N_e are found in ammonia-oxidizing archaea and bacteria from marine environments, which tend to have lower half-saturation concentrations than isolates from soil (18). Our scaling relationship Eq. **4** suggests that this ordering can arise from the smaller effective population size N_e for spatially structured environments like soil.

The other important feature of Eq. 4 is the dependence of the evolved half-saturation concentration K_{evo} on the resource concentration R_0. For a fixed effective population size N_e, there is an optimal value of R_0 that minimizes the evolved concentration K_{evo} (*Left Insets* of *SI Appendix*, Fig. S21 *A* and *B*), just as we observed for selection on individual mutations (*SI Appendix*, Fig. S17). We note that for sufficiently low values of the effective population size N_e, genetic drift is stronger than selection on any mutation κ (*SI Appendix*, Fig. S20*A*), and so the half-saturation concentration K evolves neutrally (gray region in Fig. 5*B*).

In contrast to batch dynamics, selection under chemostat dynamics does not depend on the half-saturation concentration K itself (*SI Appendix*, section S9). Intuitively, this is because reductions in K cause the environmental resource concentration to decrease proportionally (*SI Appendix*, section S5) such that the growth rate remains constant. Not only does this keep a constant strength of selection on new mutations, but the effective population size will actually increase as K evolves lower, making beneficial mutations even easier to fix. Therefore, selection–drift balance never occurs for K under chemostat dynamics; the half-saturation concentration K will continue to evolve downward until adaptation is limited by the supply of mutations or other factors (*Discussion*). Note that selection–drift balance also does not occur for mutations to the maximum growth rate g^{max} under either batch or chemostat dynamics since selection does not depend on the absolute magnitude of growth rate (*SI Appendix*, sections S8 and S9).

Population Dynamics Can Decouple the Evolved Half-Saturation Concentration from the Resource Concentration. In general, the effective population size N_e that controls genetic drift may be shaped by a variety of demographic factors besides the census population size (65). However, in well-mixed batch cultures, N_e is primarily determined by the number of cells at the bottleneck of each transfer (69); we assume that other sources of stochasticity (such as individual cell division events) are much weaker than the sampling noise of these transfers. Therefore, the effective population size N_e is proportional to the bottleneck biomass N_0 (assuming constant biomass per cell).

Under fixed-bottleneck batch dynamics, the effective population size N_e is thus an independent parameter of the population, so that the strength of genetic drift does not depend on the resource concentration (*SI Appendix*, Fig. S25*A*). In this case, the evolved trait K_{evo} is in approximately linear proportion to the resource concentration R_0 (Eq. **4**, Fig. 5*C*, and *SI Appendix*, Fig. S26*A*), making the evolved half-saturation concentration a biomarker of the resource's environmental concentration. This is consistent with our original speculation about the systematic differences in glucose K between *E. coli* and *S. cerevisiae*, owing to the different glucose availability in their different environments.

However, for fixed-dilution batch dynamics, the bottleneck biomass N_0, and therefore the effective population size N_e, are coupled to the resource concentration R_0 because the dilution factor D is fixed: $N_e \propto N_0 = R_0 Y/(D-1)$ (*SI Appendix*, section S3). This coupling occurs because increasing the resource concentration increases the biomass at the end of each growth cycle, but then, the fixed dilution factor means that this must also increase the biomass at the bottleneck. The scaling of N_e with R_0, though, cancels out the scaling of K_{evo} with R_0 in Eq. **4**, leading to an evolved half-saturation concentration K_{evo} that is approximately independent of the environmental concentration R_0 (Fig. 5*C* and *SI Appendix*, Fig. S26*B*). Conceptually, fixed-dilution batch dynamics do not allow the strength of selection to be tuned independently from genetic drift: The decrease in selection magnitude on K with higher resource concentration R_0 is compensated by weaker genetic drift, due to a higher effective population size N_e (*SI Appendix*, Fig. S25*B*). Thus, the population dynamics decouple the evolved half-saturation concentration of the organism from the environmental concentration.

This has major consequences for interpreting empirical variation. We predict the evolved half-saturation concentration K_{evo} for *E. coli* on glucose as a function of glucose concentration R_0 in Fig. 5*C*, using parameters estimated from the LTEE (*SI Appendix*, Fig. S27). On the same plot, we show a histogram of all measured glucose K values for *E. coli* (from Fig. 2*B*) on the right vertical axis. We see that, under fixed-bottleneck batch dynamics, we would expect *E. coli* to have evolved in glucose concentrations above 100 μM to account for the observed half-saturation concentrations. However, under fixed-dilution batch dynamics, the evolved half-saturation concentration depends so

Downloaded from https://www.pnas.org by LIB4RI: EAWAG-EMPA SERIALS DEPARTMENT on March 6, 2023 from IP address 152.88.31.155.

weakly on the environmental concentration that almost any concentration of glucose is possible to explain the data.

Discussion

Modeling Insights to Interpret Half-Saturation Data. Since it is often difficult to measure resource concentrations and population dynamics in natural environments, can we use the evolved half-saturation concentration K as a biomarker to infer them? This logic is often implicit in environmental studies, which attempt to draw conclusions about the environmental conditions of an isolate based on its abilities to grow at different resource concentrations (16–19). However, our model shows that it is not as simple as assuming the half-saturation concentration K for a resource is proportional to its concentration in the environment since that proportionality is altered by the population dynamics, at least through the effective population size N_e (Eq. **4**). In particular, this proportionality is confounded in the case of fixed-dilution batch dynamics, where the evolved half-saturation concentration K is largely independent of the resource concentration R_0 (Fig. 5*C*).

Under fixed-bottleneck batch dynamics, though, the linear scaling of K with R_0 does approximately hold. In this case, one can compare two populations with unknown but identical effective population sizes N_e and mutation effects κ; for example, two isogenic populations located at different points along a resource gradient. In this case, one can calculate the ratio of evolved half-saturation concentrations K_{evo} for the two populations to estimate the ratio of resource concentrations. But in many scenarios, one might not even know the type of bottlenecks the population is experiencing. To classify the population dynamics as fixed-bottleneck or fixed-dilution, one could correlate a set of evolved concentrations K_{evo} with their different resource concentrations R_0; a strong linear correlation would support fixed-bottleneck batch dynamics, while little to no correlation would indicate chemostat or fixed-dilution batch dynamics.

Role of the Mutation Supply in Shaping Evolved Half-Saturation Concentrations. We have focused on the role of selection–drift balance as a null model for the evolved variation in half-saturation concentrations since the competition between selection and genetic drift is a universal feature of all evolving populations. In doing so, we have assumed that the supply of mutations on K is constant, but real populations will at some point run out of beneficial mutations on the trait value K, potentially reaching this mutation–selection balance before selection–drift balance (70). Many mutations will also be pleiotropic, affecting both the half-saturation concentration K and the maximum growth rate g^{max} (as well as possibly other traits) simultaneously. The correlation between pleiotropic effects on both traits is important: If pleiotropy is synergistic, so that mutations that decrease K also tend to increase g^{max}, the population might evolve lower K than otherwise expected since its selection is enhanced by additional selection on g^{max}. On the other hand, if there is a tradeoff between K and g^{max}, the population might evolve higher K if its selection is outweighed by selection for higher g^{max}. Indeed, this is what appears to have happened in the LTEE, where K for glucose actually increased over the first 2,000 generations but that was offset by a stronger improvement in the maximum growth rate g^{max} (23).

Such a tradeoff between K and g^{max} is interesting both for its consequences on the stochiometric composition of community biomass (49, 72) as well as from an evolutionary point of view since the population can then diversify into stably coexisting lineages. While there is significant theoretical work on this hypothesis (25–28), it has limited empirical evidence. Some of these previous studies claiming tradeoffs found them only in parameters for the Michaelis–Menten model of resource uptake (27, 28, 30, 49, 73), which we and others have shown are not equivalent to parameters of the Monod model of growth (*SI Appendix*, Fig. S12) (37, 39). In the larger set of data we have collected in this work (Fig. 3*F*), we find no compelling evidence of a correlation; *E. coli* shows a weak but insignificant tradeoff, while *S. cerevisiae* shows a slight synergy (74).

Interpretation of this tradeoff (or lack thereof) is also complicated by the sample of strains and environmental conditions being considered. For the tradeoff to affect the evolved half-saturation concentration as we have discussed, the tradeoff must exist across the entire spectrum of spontaneous mutations available to an organism (i.e., there is an underlying physiological constraint). This has also been the underlying assumption of previous models on this topic (25–28). Testing this would require distribution of K and g^{max} values over a large mutant library in a single environment, which has not been measured to our knowledge. An experimental study in *E. coli* (31) reports a tradeoff between half-saturation concentration K for maltotriose and maximum growth rate g^{max}, but this screen was restricted to mutations in the single gene lamB, which may not be representative of genome-wide mutations. Detecting a genome-wide trade-off is further complicated by the fact that even in the absence of an underlying correlation in mutation effects, such a tradeoff could still emerge across clones within a rapidly evolving population, at least transiently (75, 76). Further systematic measurements of these traits within and between populations will be necessary to resolve the issue of a tradeoff in the future.

Other Factors Shaping Evolved Half-Saturation Concentrations. Besides mutation supply, there are other phenomena that may lead to different evolved outcomes for the half-saturation concentration K. One important assumption in our model is that we consider only a single resource, whereas real populations are dependent on several resources (77), including those from biotic sources such as cross-feeding and predation. Some of these resources may be rarely or never limiting, and therefore, their half-saturation concentrations K will evolve only as byproducts of selection on mutations for other traits. In this sense, many observed half-saturation values may actually be spandrels, an evolutionary term (defined in analogy with the architectural structure) for traits that evolve for reasons other than direct selection (78). Selection for other traits may occur simply because competition in natural environments is likely more complex and could include lag phases (51) and other strategies for low-resource survival (5, 79–81). On the other hand, multiple resources could also be simultaneously colimiting (32, 33). While we have shown how colimitation under measurement conditions affects estimates of g^{max} and K (*SI Appendix*, section S1), the effect of colimitation, as well as more complex sources of nutrients such as cross-feeding and predation, on the evolution of these traits remains an important problem for future work.

We can predict the consequences of relaxing other assumptions in our model as well. For example, simultaneous competition of multiple mutations (clonal interference) generally reduces the efficacy of selection (82, 83), which would make it more likely to evolve higher half-saturation concentrations than what we predict from SSWM dynamics. Another assumption in our model is that the population under batch dynamics always grows until

Downloaded from https://www.pnas.org by LIB4RI: EAWAG-EMPA SERIALS DEPARTMENT on March 6, 2023 from IP address 152.88.31.155.

complete exhaustion of the resources during each cycle, but earlier transfers could reduce the amount of growth occurring during deceleration, which would reduce selection on the half-saturation K. However, the population may adapt its maximum growth rate to simply saturate earlier and restore selection on its deceleration phase. Finally, populations may also have higher than expected K values if they simply have not had enough time to reach selection–drift balance, which takes a timescale of order N_e generations (*SI Appendix*, Fig. S22) (84).

Population Dynamics Are Essential for Understanding Microbial Ecology. Broadly speaking, our results provide a valuable example of how ecological traits are influenced by factors other than abiotic environmental features. In particular, we have shown how population dynamics can confound our naive expectations for the evolutionary fate of such traits. While here we have focused on the role of genetic drift, other potentially important factors include mutation supply, pleiotropy, recombination, and spatial structure. Altogether, our results mean that the half-saturation concentration K may not be a reliable biomarker of environmental resource concentrations. This does not mean that K evolves independently of the environment, however. Rather, it is linked to additional environmental processes like the bottleneck between growth cycles. To understand the systematic differences between species, we need to know not only the resource concentrations they have evolved in but also which type of population dynamics best reflects the time scales of growth, death, and resource supply in their environment of origin.

Materials and Methods

Literature Survey of Measured Growth Rate Dependence on Resources. We collected 247 measurements of Monod model parameters (K and g^{max}; Eq. **1**) through a targeted literature search that included prior surveys and reviews (41, 43), the phytoplankton trait database (130 data points) by Edwards et al. (44), as well as original research papers. In all but two cases, we traced data from surveys and reviews back to their original papers, which we report in Dataset S1, Sheet 1. We included only experiments that directly measured population growth rates, rather than nutrient uptake rates or respiration. We excluded measurements where the actual limiting resource was unclear, such as measurements in rich medium with added glucose. Where possible, we checked the raw data of growth rate over resource concentrations to determine whether the focal resource concentration was measured up to saturation and had sufficient sampling of concentrations around K. For a subset of measurements of *E. coli* on glucose, we also checked for the concentration of a nitrogen source to determine the relative impact of colimitation (Dataset S1, Sheet 2 and *SI Appendix*, section S1). If the original K value was reported as weight per volume, we converted these into units of micromolar (μM) using the calculated molecular weight of the compound's chemical formula. We preserved significant digits from the original studies. See Dataset S1 for more details.

Models of Population Dynamics. We mathematically model population dynamics using systems of ordinary differential equations for the wild-type and mutant biomasses as well as the extracellular resource concentration (*SI Appendix*, sections S3 and S5). We numerically integrate these equations using standard algorithms in Scipy (85) (*SI Appendix*, section S4).

Data, Materials, and Software Availability. Data from the literature survey of Monod growth traits (Dataset S1) has been deposited in Dryad, https://doi.org/10.5061/dryad.866t1g1tr. All methods and mathematical results to reproduce the analysis are included in the *SI Appendix*.

ACKNOWLEDGMENTS. J.W.F. and M.M. were supported by an Ambizione grant from the Swiss National Science Foundation (PZ00P3_180147). NAH was supported by the Principles of Microbial Ecosystems collaboration of the Simons Foundation (grant ID 542379) and an ETH Zurich Career Seed Grant (SEED-26 21-2). We thank Ayush Pathak for a critical reading of the manuscript.

Author affiliations: [a]Institute of Integrative Biology, Department of Environmental Systems Science, Swiss Federal Institute of Technology (ETH Zurich), 8092 Zurich, Switzerland; [b]Department of Environmental Microbiology, Swiss Federal Institute of Aquatic Science and Technology (Eawag), 8600 Dübendorf, Switzerland; and [c]Center for Advanced Biotechnology and Medicine, Department of Biochemistry and Molecular Biology, Robert Wood Johnson Medical School, Rutgers University, Piscataway, NJ 08854

1. M. Schaechter, J. L. Ingraham, F. C. Neidhardt, *Microbe* (ASM Press, Washington, DC, 2006).
2. T. E. Shehata, A. G. Marr, Effect of nutrient concentration on the growth of *Escherichia coli*. *J. Bacteriol.* **107**, 210–216 (1971).
3. N. S. Panikov, *Microbial Growth Kinetics* (Chapman & Hall, London, 1995).
4. D. L. Kirchman, Growth rates of microbes in the oceans. *Ann. Rev. Mar. Sci.* **8**, 285–309 (2016).
5. J. S. Poindexer, *Oligotrophy* (Springer, US, pp. 63–89. 1981).
6. N. Fierer, M. A. Bradford, R. B. Jackson, Toward an ecological classification of soil bacteria. *Ecology* **88**, 1354–1364 (2007).
7. J. Monod, The growth of bacterial cultures. *Ann. Rev. Microbiol.* **3**, 371–394 (1949).
8. A. L. Koch, The adaptive responses of *Escherichia coli* to a feast and famine existence. *Adv. Microb. Physiol.* **6**, 147–217 (1971).
9. D. K. Button, Kinetics of nutrient-limited transport and microbial growth. *Microbiol. Rev.* **49**, 270–279 (1985).
10. D. Tilman, *Resource Competition and Community Structure* (Princeton University Press, Princeton, NJ, 1982).
11. T. E. Miller *et al*., A critical review of twenty years' use of the resource-ratio theory. *Am. Nat.* **165**, 439–448 (2005).
12. J. R. Bernhardt *et al*., The evolution of competitive ability for essential resources. *Philos. Trans. R. Soc. B: Biol. Sci.* **375**, 20190247 (2020).
13. J. P. Grover, *Resource Competition* (Springer, US, 1997).
14. E. Marañón *et al*., Resource supply overrides temperature as a controlling factor of marine phytoplankton growth. *PLOS One* **9**, e99312 (2014).
15. E. A. Mousing, K. Richardson, M. Ellegaard, Global patterns in phytoplankton biomass and community size structure in relation to macronutrients in the open ocean. *Limnol. Oceanogr.* **63**, 1298–1312 (2018).
16. W. Martens-Habbena, P. M. Berube, H. Urakawa, J. R. de la Torre, D. A. Stahl, Ammonia oxidation kinetics determine niche separation of nitrifying archaea and bacteria. *Nature* **461**, 976–979 (2009).
17. J. I. Prosser, N. W. Graeme, Archaeal and bacterial ammonia-oxidisers in soil: The quest for niche specialisation and differentiation. *Trends Microbiol.* **20**, 523–531 (2021).
18. D. K. Kits *et al*., Kinetic analysis of a complete nitrifier reveals an oligotrophic lifestyle. *Nature* **549**, 269–272 (2017).
19. M. Y. Jung *et al*., Ammonia-oxidizing archaea possess a wide range of cellular ammonia affinities. *ISME J.* **16**, 272–283 (2022).
20. D. Dykhuizen, D. Hartl, Evolution of competitive ability in *Escherichia coli*. *Evolution* **35**, 581 (1981).
21. K. Kovářová, Ph.D. thesis (ETH Zurich, Zurich, Switzerland) (1996).
22. J. Adams, C. Paquin, P. W. Oeller, L. W. Lee, Physiological characterization of adaptive clones in evolving populations of the yeast *Saccharomyces cerevisiae*. *Genetics* **110**, 173–185 (1985).
23. F. Vasi, M. Travisano, R. E. Lenski, Long-term experimental evolution in *Escherichia coli*. II. Changes in life-history traits during adaptation to a seasonal environment. *Am. Nat.* **144**, 432–456 (1994).
24. S. F. M. Hart, C. C. Chen, W. Shou, Pleiotropic mutations can rapidly evolve to directly benefit self and cooperative partner despite unfavorable conditions. *eLife* **10**, e57838 (2021).
25. F. M. Stewart, B. R. Levin, Partitioning of resources and the outcome of interspecific competition: A model and some general considerations. *Am. Nat.* **107**, 171–198 (1973).
26. A. M. Dean, Protecting haploid polymorphisms in temporally variable environments. *Genetics* **169**, 1147–1156 (2005).
27. R. E. Beardmore, I. Gudelj, D. A. Lipson, L. D. Hurst, Metabolic trade-offs and the maintenance of the fittest and the flattest. *Nature* **472**, 342–346 (2011).
28. M. T. Wortel, Evolutionary coexistence in a fluctuating environment by specialization on resource level. BioRxiv preprint (2021), 2021.05.18.444718. Accessed 5 October 2021.
29. K. W. Wirtz, A generic model for changes in microbial kinetic coefficients. *J. Biotechnol.* **97**, 147–162 (2002).
30. E. Litchman, C. A. Klausmeier, O. M. Schofield, P. G. Falkowski, The role of functional traits and trade-offs in structuring phytoplankton communities: Scaling from cellular to ecosystem level. *Ecol. Lett.* **10**, 1170–1181 (2007).
31. J. R. Meyer, I. Gudelj, R. Beardmore, Biophysical mechanisms that maintain biodiversity through trade-offs. *Nat. Commun.* **6**, 6278 (2015).
32. M. A. Saito, T. J. Goepfert, J. T. Ritt, Some thoughts on the concept of colimitation: Three definitions and the importance of bioavailability. *Limnol. Oceanogr.* **53**, 276–290 (2008).
33. S. W. Harpole *et al*., Nutrient co-limitation of primary producer communities. *Ecol. Lett.* **14**, 852–862 (2011).
34. D. K. Button, Affinity of organisms for substrate. *Limnol. Oceanogr.* **31**, 435–456 (1986).
35. F. P. Healey, Slope of the Monod equation as an indicator of advantage in nutrient competition. *Microb. Ecol.* **5**, 281–286 (1980).

Downloaded from https://www.pnas.org by LIB4RI: EAWAG-EMPA SERIALS DEPARTMENT on March 6, 2023 from IP address 152.88.31.155.

36. R. V. O'Neill, D. L. DeAngelis, J. J. Pastor, B. J. Jackson, W. M. Post, Multiple nutrient limitations in ecological models. *Ecol. Modell.* **46**, 147–163 (1989).
37. J. L. Snoep, M. Mrwebi, J. M. Schuurmans, J. M. Rohwer, M. J. Teixeira de Mattos, Control of specific growth rate in *Saccharomyces cerevisiae*. *Microbiology* **155**, 1699–1707 (2009).
38. S. Sharma, R. Steuer, Modelling microbial communities using biochemical resource allocation analysis. *J. R. Soc. Inter.* **16**, 20190474 (2019).
39. D. Tilman, S. S. Kilham, Phosphate and silicate growth and uptake kinetics of the diatoms Asterionella formosa and Cyclola meneghiniana in batch and semicontinuous culture. *J. Phycol.* **12**, 375–383 (1976).
40. F. M. M. Morel, Kinetics of nutrient uptake and growth in phytoplankton. *J. Phycol.* **23**, 137–150 (1987).
41. J. Owens, J. Legan, Determination of the Monod substrate saturation constant for microbial growth. *FEMS Microbiol. Lett.* **46**, 419–432 (1987).
42. H. W. Jannasch, Growth characteristics of heterotrophic bacteria in seawater. *J. Bacteriol.* **95**, 722–723 (1968).
43. K. Kovárová-Kovar, T. Egli, Growth kinetics of suspended microbial cells: From single-substrate-controlled growth to mixed-substrate kinetics. *Microbiol. Mol. Biol. Rev.* **62**, 646–666 (1998).
44. K. F. Edwards, C. A. Klausmeier, E. Litchman, Nutrient utilization traits of phytoplankton. *Ecology* **96**, 2311–2311 (2015).
45. R. Milo, R. Phillips, *Cell Biology by the Numbers* (Garland Science, Taylor Francis Group, 2016).
46. T. Ferenci, Growth of bacterial cultures 50 years on: Towards an uncertainty principle instead of constants in bacterial growth kinetics. *Res. Microbiol.* **150**, 431–38 (1999).
47. H. F. Liu *et al*., Sugar and acid concentrations in 98 grape cultivars analyzed by principal component analysis. *J. Sci. Food Agric.* **86**, 1526–36 (2006).
48. Z. T. Dame *et al*., The human saliva metabolome. *Metabolomics* **11**, 1864–1883 (2015).
49. E. Litchman, K. F. Edwards, C. A. Klausmeier, Microbial resource utilization traits and trade-offs: Implications for community structure, functioning, and biogeochemical impacts at present and in the future. *Front. Microbiol.* **6** (2015).
50. C. Luis-Miguel, On measuring selection in experimental evolution. *Biol. Lett.* **7**, 210–213 (2011).
51. M. Manhart, B. V. Adkar, E. I. Shakhnovich, Trade-offs between microbial growth phases lead to frequency-dependent and non-transitive selection. *Proc. R. Soc. B: Biol. Sci.* **285** (2018).
52. M. J. Behrenfeld *et al*., Annual boom-bust cycles of polar phytoplankton biomass revealed by space-based lidar. *Nat. Geosci.* **10**, 118–122 (2017).
53. D. M. Needham *et al*., Short-term observations of marine bacterial and viral communities: Patterns, connections and resilience. *ISME J.* **7**, 1274–1285 (2013).
54. T. N. Enke *et al*., Modular assembly of polysaccharide-degrading marine microbial communities. *Curr. Biol.* **29** (2019).
55. J. Cremer, M. Arnoldini, T. Hwa, Effect of water flow and chemical environment on microbiota growth and composition in the human colon. *Proc. Natl. Acad. Sci. U.S.A.* **114**, 6438–43 (2017).
56. J. E. Barrick, R. E. Lenski, Genome dynamics during experimental evolution. *Nat. Rev. Genet.* **14**, 827–839 (2013).
57. S. Dutkiewicz, M. J. Follows, J. G. Bragg, Modeling the coupling of ocean ecology and biogeochemistry. *Global Biogeochem. Cycles* **23** (2009).
58. R. E. Lenski, M. R. Rose, S. C. Simpson, S. C. Tadler, Long-term experimental evolution in *Escherichia coli*. I. Adaptation and divergence during 2,000 generations. *Am. Nat.* **138**, 1315–1341 (1991).
59. J. H. Gillespie, Molecular evolution over the mutational landscape. *Evolution* **38**, 1116–1129 (1984).
60. A. Bren, Y. Hart, E. Dekel, D. Koster, U. Alon, The last generation of bacterial growth in limiting nutrient. *BMC Syst. Biol.* **7**, 27 (2013).
61. T. Ferenci, Adaptation to life at micromolar nutrient levels: The regulation of Escherichia Coli glucose transport by endoinduction and camp. *FEMS Microbiol. Rev.* **18**, 301–317 (1996).
62. J. W. Lengeler, Carbohydrate transport in bacteria under environmental conditions, a black box? *Antonie van Leeuwenhoek* **63** (1993).
63. J. F. Crow, M. Kimura, *An Introduction to Population Genetics Theory* (Harper and Row, New York, 1970).
64. W. J. Ewens, *Mathematical Population Genetics* (Springer-Verlag, New York, 2004).
65. B. Charlesworth, Effective population size and patterns of molecular evolution and variation. *Nat. Rev. Genet.* **10**, 195–205 (2009).
66. O. Hallatschek, P. Hersen, S. Ramanathan, D. R. Nelson, Genetic drift at expanding frontiers promotes gene segregation. *Proc. Natl. Acad. Sci. U.S.A.* **104**, 19926–19930 (2007).
67. M. Shpak, Selection against demographic stochasticity in age-structured populations. *Genetics* **177**, 2181–2194 (2007).
68. J. H. Gillespie, Natural selection for within-generation variance in offspring number II. Discrete haploid models. *Genetics* **81**, 403–413 (1975).
69. M. Kimura, *The Neutral Theory of Molecular Evolution* (Cambridge University Press, Cambridge, 1983).
70. A. W. R. Serohijos, E. I. Shakhnovich, Merging molecular mechanism and evolution: Theory and computation at the interface of biophysics and evolutionary population genetics. *Curr. Opin. Struct. Biol.* **26**, 84–91 (2014).
71. M. Lynch, K. Hagner, Evolutionary meandering of intermolecular interactions along the drift barrier. *Proc. Natl. Acad. Sci. U.S.A.* **112**, E30–38 (2015).
72. K. J. Flynn *et al*., Is the growth rate hypothesis applicable to microalgae?*J. Phycol.* **46**, 1–12 (2010).
73. K. Elbing *et al*., Role of hexose transport in control of glycolytic flux in *Saccharomyces cerevisiae*. *Appl. Environ. Microbiol.* **70**, 5323–5330 (2004).
74. N. Ziv, M. L. Siegal, D. Gresham, Genetic and nongenetic determinants of cell growth variation assessed by high-throughput microscopy. *Mol. Biol. Evol.* **30**, 2568–2578 (2013).
75. K. Gomez, J. Bertram, J. Masel, Directional selection rather than functional constraints can shape the G matrix in rapidly adapting asexuals. *Genetics* **211**, 715–729 (2019).
76. J. Lin, M. Manhart, A. Amir, Evolution of microbial growth traits under serial dilution. *Genetics* **215** (2020).
77. M. Kaspari, J. S. Powers, Biogeochemistry and geographical ecology: Embracing all twenty-five elements required to build organisms. *Am. Nat.* **188**, S62–S73 (2016).
78. S. J. Gould, R. C. Lewontin, The spandrels of San Marco and the Panglossian paradigm: A critique of the adaptationist programme. *Proc. R. Soc. B* **205**, 581–598 (1979).
79. A. L. Koch, Oligotrophs versus copiotrophs. *BioEssays* **23**, 657–661 (2001).
80. R. Cavicchioli, M. Ostrowski, F. Fegatella, A. Goodchild, N. Guixa-Boixereu, Life under nutrient limitation in oligotrophic marine environments: An eco/physiological perspective of Sphingopyxix alaskensis (Formerly Sphingomonas alaskensis). *Microb. Ecol.* **45**, 203–217 (2003).
81. J. Grote *et al*., Streamlining and core genome conservation among highly divergent members of the SAR11 clade. *mBio* **3**, e00252–12 (2012).
82. P. J. Gerrish, R. E. Lenski, The fate of competing beneficial mutations in an asexual population. *Genetica* **102** (103), 127–144 (1998).
83. S. Schiffels, G. J. Szollosi, V. Mustonen, M. Lässig, Emergent neutrality in adaptive asexual evolution. *Genetics* **189**, 1361–1375 (2011).
84. M. Kimura, T. Ohta, The average number of generations until fixation of a mutant gene in a finite population. *Genetics* **61**, 763–771 (1969).
85. P. Virtanen *et al*., SciPy 1.0 fundamental algorithms for scientific computing in Python. *Nat. Methods* **17**, 261–272 (2020).

Downloaded from https://www.pnas.org by LIB4RI: EAWAG-EMPA SERIALS DEPARTMENT on March 6, 2023 from IP address 152.88.31.155.